Short-time diffusion of charge-stabilized colloidal particles: generic features
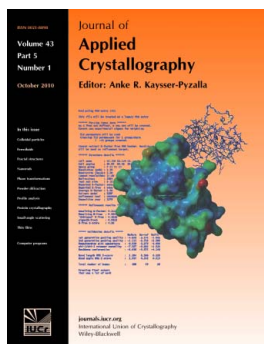
Marco Heinen, Peter Holmqvist, Adolfo J. Banchio and Gerhard Nägele

Many research topics in condensed matter research, materials science and the life sciences make use of crystallographic methods to study crystalline and non-crystalline matter with neutrons, X-rays and electrons. Articles published in the *Journal of Applied Crystallography* focus on these methods and their use in identifying structural and diffusion-controlled phase transformations, structure–property relationships, structural changes of defects, interfaces and surfaces, *etc.* Developments of instrumentation and crystallographic apparatus, theory and interpretation, numerical analysis and other related subjects are also covered. The journal is the primary place where crystallographic computer program information is published.

Crystallography Journals Online is available from **journals.iucr.org**

Short-time diffusion of charge-stabilized colloidal particles: generic features

Marco Heinen,[a] Peter Holmqvist,[a] Adolfo J. Banchio[b] and Gerhard Nägele[a]*

[a]Institut für Festkörperforschung, Forschungszentrum Jülich, D-52425 Jülich, Germany, and
[b]FaMAF, Universidad Nacional de Córdoba, and IFEG-CONICET, Ciudad Universitaria, 5000 Córdoba, Argentina. Correspondence e-mail: g.naegele@fz-juelich.de

Analytical theory and Stokesian dynamics simulations are used in conjunction with dynamic light scattering to investigate the role of hydrodynamic interactions in short-time diffusion in suspensions of charge-stabilized colloidal particles. The particles are modeled as solvent-impermeable charged spheres, repelling each other *via* a screened Coulomb potential. Numerical results for self-diffusion and sedimentation coefficients, as well as hydrodynamic and short-time diffusion functions, are compared with experimental data for a wide range of volume fractions. The theoretical predictions for the generic behavior of short-time properties obtained from this model are shown to be in full accord with experimental data. In addition, the effects of microion kinetics, nonzero particle porosity and residual attractive forces on the form of the hydrodynamic function are estimated. This serves to rule out possible causes for the strikingly small hydrodynamic function values determined in certain synchrotron radiation experiments.

1. Introduction

Dispersions of charged colloidal particles undergoing correlated Brownian motion form a particularly important class of soft-matter systems ubiquitously encountered in the chemical industry, food science and biology (Pusey, 1991; Nägele, 1996; Bowen & Mongruel, 1998; Retailleau *et al.*, 1999; Bowen *et al.*, 2000; Riese *et al.*, 2000; Koenderink *et al.*, 2003; Gapinski *et al.*, 2005; Prinsen & Odijk, 2007). The calculation of diffusion transport properties for these systems is challenging since one needs to cope, in addition to direct electrosteric and van der Waals interparticle forces, with the solvent-mediated hydrodynamic interactions (HIs). The latter type of interaction is long-ranged and non-pairwise additive in nondilute systems.

In the present paper, using analytical theory, simulation and light scattering, we discuss generic features of diffusion in fluid-like ordered suspensions of charge-stabilized colloidal spheres, as observed on a short-time colloidal scale. The most frequently used experimental methods to study the dynamics of charge-stabilized systems are dynamic light scattering (DLS) and X-ray photon correlation spectroscopy (XPCS). In both methods, the dynamic structure factor, $S(q, t)$, is determined as a function of scattering wavenumber q and correlation time t. At short times, $S(q, t)$ decays exponentially according to (Pusey, 1991)

$$S(q, t) \propto \exp[-q^2 D(q)t]. \tag{1}$$

The short-time diffusion function (Nägele, 1996),

$$D(q) = d_0 H(q)/S(q), \tag{2}$$

is determined by the ratio of the positive-definite hydrodynamic function $H(q)$ and the static structure factor $S(q)$. At zero particle concentration, $D(q)$ reduces to the single-particle diffusion coefficient d_0. The hydrodynamic function, $H(q)$, obtained experimentally by the short-time measurement of $D(q)$ in combination with a static scattering experiment determining $S(q)$, quantifies the influence of the HIs on colloidal short-time diffusion and sedimentation. Without HIs, $H(q)$ is a constant function equal to one. Any q dependence of $H(q)$ reflects the influence of HIs. In the limit of large wavenumbers compared to the position, q_m, of the principal peak of $S(q)$, the function $H(q)$ becomes equal to the normalized short-time self-diffusion coefficient, d_S/d_0, which is smaller than one when HIs are significant. In the limit of $q \to 0$, $H(q)$ reduces to the sedimentation coefficient $K = U_S/U_0$. Here, U_S is the mean sedimentation velocity of particles in a uniform suspension subject to a weak constant force field, and U_0 is the single-sphere sedimentation velocity under the same force field. For an arbitrary value of q, $H(q)$ has the meaning of a generalized sedimentation (or mobility) coefficient, linearly relating a spatially periodic force field of wavelength $2\pi/q$ acting on the particles to the resulting spatially periodic particle drift velocities. The most significant value of $H(q)$ is its principal peak height, $H(q_m)$, attained at a wavenumber that almost coincides with the position, q_m, of the principal peak of $S(q)$. The value of $H(q_m)$ relates to the short-time relaxation of density fluctuations of wavelength $2\pi/q_m$, comparable in size

to the radius of the dynamic cage of next-neighbor particles formed around each particle.

A theoretical discussion of $H(q_m)$ for charged spheres as a function of the particle volume fraction φ was given recently by Gapinski *et al.* (2010). Therein, it was shown that, because of the increasing strength of near-field HIs with increasing concentration, $H(q_m)$ behaves non-monotonically in φ at low salinity, showing an initial increase towards its maximal value larger than one, followed by a decline for further enlarged φ to values that can be smaller than one. This behavior differs from that of the sedimentation and short-time self-diffusion coefficients, which both decrease monotonically with increasing φ. Gapinski *et al.* (2010) provided in addition the universal limiting freezing line for $H(q_m)$, which leads to a useful map of hydrodynamic function peak values attainable in the fluid regime.

Our calculations of short-time diffusion properties are based on the one-component macroion fluid (OMF) model, which describes the colloidal particles as uniformly charged spheres with stick hydrodynamic boundary conditions on their surfaces (Banchio & Nägele, 2008). The spheres interact by a screened Coulomb potential of Derjaguin–Landau–Verwey–Overbeek (DLVO) type. The accuracy of two analytical methods to calculate short-time properties is assessed by comparison with results from numerically accurate, but computationally expensive, accelerated Stokesian dynamics (ASD) simulations (Banchio & Brady, 2003; Gapinski *et al.*, 2005; Banchio & Nägele, 2008), and with DLS data on charged silica spheres in a toluene–ethanol mixture.

The first analytical method is the $\delta\gamma$ scheme introduced by Beenakker & Mazur (1984). It accounts in an approximate way for many-body HI contributions, but ignores higher-order near-field HI contributions and lubrication effects. The $\delta\gamma$ scheme gives qualitatively good results for $H(q)$ throughout the liquid colloid phase. It can be further improved in its prediction of $H(q)$ when its microstructure-independent self-part is replaced by an accurate simulation expression (Gapinski *et al.*, 2005; Banchio & Nägele, 2008).

The second analytical method, referred to as the fully pairwise additive (full PA) approximation, completely accounts for HIs on the pairwise level, but it ignores three-body and higher-order hydrodynamic contributions. This method is exact for very low values of φ, where HIs are pairwise additive. Therefore, by comparison with ASD simulation data for the considered short-time property, the full PA scheme allows us to infer the importance of three-body and higher-order HI contributions. Unlike the $\delta\gamma$ scheme, the full PA method is bound to fail at higher concentrations because of its complete neglect of many-body HIs. Both analytical methods require $S(q)$ or, alternatively, its real-space analog, the radial distribution function $g(r)$, as the only input. The static input is computed using an improved version (Heinen *et al.*, 2010) of the computationally very efficient penetrating background-corrected rescaled mean spherical approximation (PBRMSA) scheme (Snook & Hayter, 1992), discussed further below. The high accuracy of this largely unknown analytical scheme is demonstrated by comparison with Monte

Carlo (MC) simulations, and results from the accurate but numerically far more elaborate Rogers–Young (RY) scheme (Rogers & Young, 1984).

The theoretical and simulation results for the short-time properties are compared with our (dynamic) light scattering data on low-salinity suspensions of charged silica spheres, and with scattering data on charge-stabilized systems by some other groups. The results presented in this paper serve to highlight generic features of short-time diffusion properties of charged particles, in comparison to those of neutral hard spheres, and to explore the range of applicability of useful analytical expressions describing a non-analytical φ dependence of d_S, K and $H(q_m)$ for small values of φ and long-range repulsion (low salinity).

In addition, we discuss qualitatively the changes in $H(q)$ when interaction contributions not included in the OMF model are operative. We analyze the effect of short-range attractions caused, for example, by van der Waals forces, the influence of particle porosity, hydrodynamic screening and the additional dynamic friction due to the electrokinetic relaxation of the microionic cloud dragged along by each colloidal sphere. This discussion serves to scrutinize possible causes for the strikingly small values for $H(q)$ determined in synchrotron radiation experiments by Robert and collaborators (Robert, 2001, 2007; Hammouda & Mildner, 2007; Robert *et al.*, 2008; Grübel *et al.*, 2008) for certain low-salinity systems. These values are considerably smaller than those of neutral hard spheres. The findings of Robert and co-workers are incompatible not only with short-time predictions based on the OMF model but also with experimental data for all other (low-salinity) charge-stabilized systems that we are aware of, where $H(q_m)$ is found to be always larger than the peak value of hard spheres at the same φ. We correct an incorrect statement by Robert (2007) made on the equality of the self-diffusion coefficient for neutral and charged spheres.

While the present work focuses on short-time dynamics, we point here to recent DLS experiments showing that a far-reaching scaling behavior of the dynamic structure factor of neutral hard spheres (Segrè & Pusey, 1996), relating short-time to long-time dynamics, is approximately valid also for charged colloids (Holmqvist & Nägele, 2010). Short-time diffusion in charged colloids is not only an interesting topic in its own right. Such knowledge is also a prerequisite for a better understanding of the long-time dynamics.

2. Methods of calculation and experimental details

The presented analytical and computer simulation results for the short-time diffusion properties and $S(q)$ are based on the OMF model. In this simplifying model, a colloidal sphere and its cloud of neutralizing microions are described as a uniformly charged sphere of diameter σ, interacting electrostatically by an effective pair potential, $u(r)$, of DLVO type (Nägele, 1996):

$$\frac{u(r)}{k_B T} = L_B Z^2 \left[\frac{\exp(\kappa a)}{1+\kappa a}\right]^2 \frac{\exp(-\kappa r)}{r}, \quad r > \sigma = 2a. \quad (3)$$

The screening parameter, κ, is given by

$$\kappa^2 = 4\pi L_B(n|Z| + 2n_s)/(1 - \varphi), \qquad (4)$$

where n is the colloid number density, n_s is the number density of added 1–1 electrolyte and $\varphi = (4\pi/3)na^3$ is the colloid volume fraction of spheres with radius a. Furthermore, Z is the effective particle charge in units of the elementary charge e, and $L_B = e^2/(\varepsilon k_B T)$ is the Bjerrum length of the suspending Newtonian solvent of dielectric constant ε at temperature T, where k_B is the Boltzmann constant. We assume here that the counter-ions released from the colloid surfaces are monovalent. The factor $1/(1 - \varphi)$ is frequently introduced to correct for the free volume accessible to the microions. Hydrodynamically, the colloidal particles are treated as nonpermeable rigid spheres with stick boundary conditions on their surfaces. The OMF model captures essential features of charge-stabilized suspensions, for systems where the short-range van der Waals forces can be neglected.

As mentioned above, we use two efficient analytical methods to calculate $H(q)$ and its small- and large-q limiting values K and d_S/d_0, respectively. The zeroth-order $\delta\gamma$ method (Beenakker & Mazur, 1984) invokes a partial re-summation of the many-body HI contributions. It uses truncated hydrodynamic mobility tensors without lubrication corrections. An extensive comparison (Gapinski et al., 2005, 2007, 2009; Banchio & Nägele, 2008; Banchio et al., 2006) of the $\delta\gamma$ scheme predictions for $H(q)$ with ASD simulation results has shown that it reproduces the $H(q)$ of charge-stabilized particles quite well, to a degree even better than for neutral hard spheres where lubrication is strong, when in place of the original self-part the accurate ASD simulation result for d_S/d_0 is used so that $H(q) = d_S^{ASD}/d_0 + H_d^{\delta\gamma}(q)$. At smaller φ, one can more conveniently use the full PA scheme result for d_S. This improvement can be understood from noting that d_S is underestimated by the $\delta\gamma$ scheme, since the zeroth-order expression for d_S used here does not account for the pair structure of charged spheres. However, and most importantly, the wavenumber-dependent distinct part, $H_d(q)$, is well described by the $\delta\gamma$ scheme (Gapinski et al., 2005; Banchio & Nägele, 2008). In the following section, we exemplify the accuracy of the self-part-corrected $\delta\gamma$ scheme, in comparison to MC simulations and experimental results for $H(q)$, for the most interesting case of suspensions of strongly correlated particles at lower salt content.

The second analytical method, the full PA approximation, uses tables of numerically precise values for the two-body mobility tensors provided by Jeffrey & Onishi (1984), Kim & Mifflin (1985) and Jones & Schmitz (1988). The full PA scheme is a significant improvement over earlier two-body approximations for $H(q)$, also commonly referred to as PA schemes, where only a long-distance form of the hydrodynamic pair mobilities in terms of an (a/r) inverse pair distance expansion truncated after a few terms has been used (Nägele et al., 1994, 1995; Nägele, 1996; Watzlawek & Nägele, 1999; Robert, 2001, 2007). The full PA method becomes exact at very small φ where the HIs are truly pairwise additive. However, it neces-

sarily fails at larger φ since it disregards three-body and higher-order hydrodynamic contributions.

The static input $S(q)$, required by both analytical methods, is obtained using the PBRMSA scheme (Snook & Hayter, 1992). We have augmented this method by a simple density rescaling of the screening parameter in equation (4). This rescaling leads to very accurate structure factors, as shown recently by an extensive comparison with simulation data, and results from the RY integral equation scheme (Heinen et al., 2010). Two examples demonstrating the accuracy of the PBRMSA $S(q)$ are discussed in the following section.

Furthermore, we calculate $H(q)$ using the ASD simulation code of Banchio & Brady (2003), extended to the OMF model of charged spheres (Gapinski et al., 2005; Banchio et al., 2006; Banchio & Nägele, 2008). This elaborate simulation method accounts for many-body HIs and lubrication. The calculated hydrodynamic function exhibits a pronounced $O(N^{-1/3})$ dependence on the number, N, of particles in the basic simulation box. A finite-size scaling extrapolation procedure, originally used by Ladd (1990) for neutral spheres, is applied to extrapolate to the $H(q)$ of a macroscopically large system. The good agreement of the finite-size-corrected ASD $H(q)$ with the full PA scheme result at small volume fractions ($\varphi < 10^{-2}$), where the latter scheme becomes exact, demonstrates the validity of Ladd's finite-size scaling method for application to charged spheres. Stokesian dynamics simulations of $H(q)$ are computationally expensive even when the accelerated code is used. Therefore, fast approximate schemes such as the $\delta\gamma$ method are still in demand, in particular when various system parameters need to be varied to explore generic features.

For dilute, low-salinity systems of strongly charged particles, characterized by $q_m \propto \varphi^{1/3}$, very simple expressions with fractional exponents apply:

$$K \simeq 1 - a_s \varphi^{1/3}, \qquad (5)$$

$$d_S/d_0 \simeq 1 - a_t \varphi^{4/3}, \qquad (6)$$

$$H(q_m) \simeq 1 + p_m \varphi^{1/3}. \qquad (7)$$

These expressions have been derived using the leading-order far-field forms of the hydrodynamic mobilities (Nägele, 1996; Nägele et al., 1994, 1995; Watzlawek & Nägele, 1999). The coefficients $a_s \simeq 1.6$–1.8 and $a_t \simeq 2.5$–2.9 in the expressions for K and d_S/d_0 depend to a certain extent on the particle charge and size. The coefficient $p_m > 0$ related to $H(q_m)$ also depends on Z and κa (Gapinski et al., 2010; Banchio & Nägele, 2008). All coefficients are typically larger for more structured suspensions, signalled by a higher peak value of $S(q_m)$. As we will show, the φ interval where the expression for d_S in equation (6) applies is broader than the interval for the collective properties K and $H(q_m)$.

It will prove useful in what follows to compare the short-time results for charged colloidal spheres with those of neutral hard spheres at the same φ. Cichocki et al. (1999, 2002) derived the following virial expansion results for neutral hard spheres (HS):

$$K^{\mathrm{HS}} = 1 - 6.546\,\varphi + 21.918\,\varphi^2 + \mathcal{O}(\varphi^3), \tag{8}$$

$$d_{\mathrm{S}}^{\mathrm{HS}}/d_0 = 1 - 1.832\,\varphi - 0.219\,\varphi^2 + \mathcal{O}(\varphi^3), \tag{9}$$

valid to quadratic order in φ. These truncated virial expansion results fully account for HIs up to the three-body level.

The hydrodynamic function peak height of hard spheres is given to excellent accuracy by Banchio *et al.* (1999):

$$H^{\mathrm{HS}}(q_{\mathrm{m}}) = 1 - 1.35\varphi, \tag{10}$$

with the linear φ dependence valid up to the freezing transition concentration.

The short-time experimental data presented in this work have been obtained using DLS from fluid-ordered and nearly monodisperse suspensions of negatively charged trimethoxysilylpropyl methacrylate (TPM)-coated silica spheres (Philipse & Vrij, 1988), dispersed in an index-matching 80:20 toluene–ethanol solvent mixture at $T = 293$ K and $L_{\mathrm{B}} = 8.64$ nm. The particle radius determined by small-angle X-ray scattering (SAXS) is $a = 136$ nm and the size polydispersity is 0.06. The salinity of residual 1–1 electrolyte is below 1 μM. Monovalent counter-ions (hydrated protons) are released into the solvent from the coated silica surfaces. The studied charged silica system freezes at $\varphi \simeq 0.16$ where $S(q_{\mathrm{m}}) \simeq 3.2$. The DLS measurements were made using a light-scattering setup by the ALV-Laservertriebsgesellschaft (Langen, Germany) and an ALV-5000 multi-tau digital correlator. We

Figure 1
Normalized short-time self-diffusion coefficient, d_{S}/d_0, of a deionized suspension of charged spheres (CS, black) and hard spheres (HS, gray). Crosses: DLS data for TPM-coated charged silica spheres. Black circles and gray diamonds: ASD results for CS and HS, respectively. Solid black and gray lines: full PA theory results for CS and HS, using the PBRMSA and Percus–Yevick input for $S(q)$, respectively. Dashed black line: $1 - 2.5\varphi^{4/3}$. Dashed–dotted gray line: second-order virial result for HS. Inset: d_{S}/d_0 as predicted by the full PA scheme (lines), and by ASD simulation (symbols), with the leading-order far-field HI part for CS (black) and HS (gray), respectively, subtracted off.

carefully checked that there is no noticeable multiple scattering.

3. Results

In the following, we present our theoretical and simulation results for charged colloidal particles based on the OMF model, and compare them with our light scattering data on coated charged silica spheres and scattering data by two other groups. The results for charged colloidal spheres (CS) are compared in addition with corresponding findings for neutral hard spheres (HS), to highlight salient differences in the short-time diffusion properties which are largest when low-salinity charge-stabilized systems are considered. Therefore, only charge-stabilized systems of lower salinity are considered. For the influence of added salt on the short-time diffusion coefficients and $H(q)$ we refer to extensive ASD simulations and analytical calculations published by Gapinski *et al.* (2009, 2010), Banchio & Nägele (2008) and Banchio *et al.* (2008). Therein, it is shown that the OMF-based diffusion properties cross over monotonically, with increasing salt concentration, from their zero-salt values to those of neutral hard spheres. This expected behavior is reflected also in the static structure factor.

3.1. Self-diffusion

Fig. 1 includes the prediction by the full PA scheme for the normalized short-time self-diffusion coefficient, d_{S}/d_0, of charged and neutral hard spheres in comparison with ASD simulation results and our DLS data for TPM-coated charged silica spheres. The comparison of the full PA scheme result with the ASD data allows us to deduce quantitatively the contribution to d_{S} by the non-pairwise additive part of the HIs arising from the solvent-mediated interactions of three or more particles.

The large-q regime related to self-diffusion is usually not accessible by DLS. Therefore, using an argument put forward by Pusey (1978), we identify d_{S} approximately as $d_{\mathrm{S}} \simeq D(q^*)$ (crosses in Fig. 1), where q^* is the first wavenumber located to the right of q_{m} for which $S(q^*) = 1$ (see top part of Fig. 3). Simulations of charged and neutral spheres have shown that d_{S} is determined in this way to within 5–10% accuracy (Banchio & Nägele, 2008; Abade *et al.*, 2010*a*,*b*). A comment is in order here on an incorrect proposition by Robert (2007), who stated that one of the present authors (G. Nägele) has predicted theoretically that there is no difference in the concentration dependence of d_{S} for charged and neutral particles. Quite the contrary, Nägele and co-workers have shown for charged spheres at low salinity that $d_{\mathrm{S}}/d_0 \simeq 1 - a_{\mathrm{t}}\varphi^{4/3}$ [*cf.* equation (6)], *i.e.* d_{S} in these systems has a fractional φ dependence qualitatively different from that of hard spheres (Nägele *et al.*, 1994, 1995; Nägele, 1996). Only the self-diffusion coefficient of neutral hard spheres can be described by a regular virial series, with the first two virial coefficients given in equation (9). The correct second-order term, $-0.219\varphi^2$, in equation (9) differs even in its sign from the erroneous result, $+0.88\varphi^2$, used by Robert (2007).
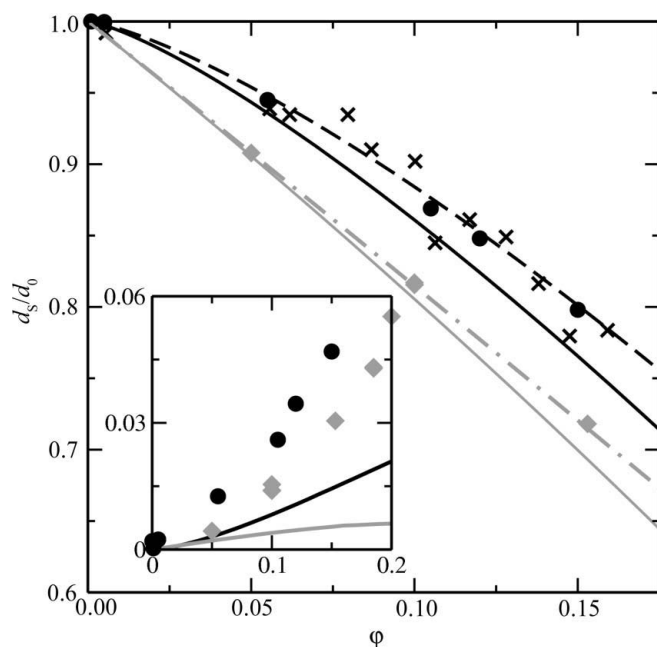
The $\varphi^{4/3}$ dependence of $d_S/d_0 - 1$ was confirmed both by the experiments of Overbeck *et al.* (1999) and by ASD simulations based on the OMF model (Banchio & Nägele, 2008). The depicted ASD data for a low-salinity system of charged spheres are overall well described by the fractional φ relation in equation (6) for $a_t \simeq 2.5$, over an extended range of volume fractions (black solid line in Fig. 1).

Considering the scatter in the charged silica sphere DLS data for d_S depicted in Fig. 1, their overall φ dependence is consistent with the ASD simulation data and the $\varphi^{4/3}$ scaling prediction. The full PA scheme overestimates the strength of the HIs in nondilute suspensions, because it does not account for the shielding of the HIs between a pair of particles by other intervening particles. This is the reason why, at intermediate and larger concentrations, the ASD and experimental data for d_S are underestimated by the full PA method. Note that the full PA scheme result for d_S/d_0 is still well described by the scaling relation in equation (6), but for a somewhat larger parameter value of $a_t \simeq 2.9$. We emphasize here that hydrodynamic shielding is a many-body HI effect, which lowers the strength but not the range of the HIs. It should not be confused, as in earlier work (Riese *et al.*, 2000), with the screening of the HIs by spatially fixed particles or boundaries that absorb momentum from the fluid, therefore causing a faster than $1/r$ decay of the flow perturbation created by a point force (Diamant, 2007).

The hydrodynamic self-mobility related to d_S is rather short-ranged, decaying like $1/r^4$ for a large separation r of two spheres. Consequently, the difference between d_S and its infinite dilution value d_0 is smaller for charged spheres than for neutral ones, since electric repulsion disfavors near-contact configurations. The inset in Fig. 1 shows d_S/d_0, as obtained by the full PA scheme and ASD simulations, respectively, but with the far-field part originating from the leading-order self-mobility part proportional to $1/r^4$ subtracted off. According to the inset, d_S is rather insensitive to the near-field two-body part of the HIs, causing a small increase in d_S only. The full PA scheme reproduces exactly the first-order virial coefficient, -1.832, of hard spheres given in equation (9). This demonstrates the high precision of the numerical tables for the hydrodynamic pair mobilities used in our full PA scheme calculations. Three-body and higher-order HI contributions come into play for $\varphi \gtrsim 0.08$, with an enlarging influence on d_S originating from hydrodynamic shielding.

3.2. Sedimentation

In principle, one needs to distinguish between the short-time and the long-time sedimentation coefficients, but the latter is smaller than the first by at most a few percent. The two coefficients are practically equal in dilute systems where the two-body HI part dominates.

Fig. 2 includes theoretical, simulation and experimental results for the (short-time) sedimentation coefficient, K, of homogeneous systems for charged and neutral spheres. The key message conveyed by this figure is the qualitative difference in the φ dependence of K for charged and neutral

particles. This difference is more pronounced than that for the self-diffusion coefficient discussed earlier. Charged spheres sediment more slowly than uncharged ones since near-contact configurations are disfavored. Thus, stronger laminar friction takes place between the back-flowing solvent and the solvent layers dragged along with the settling spheres because of the stick hydrodynamic boundary condition. The solvent back-flow is created by a pressure gradient directed towards the container bottom, which balances the nonzero buoyancy-corrected total gravitational force on the spheres.

At smaller φ and low salinity, K is well described by the nonlinear expression $1 - a_s\varphi^{1/3}$ in equation (5), with a coefficient $a_s \simeq 1.6$–1.8 depending to some extent on the strength of the electrostatic pair interactions. The exponent $1/3$ arises from the two-body far-field part of the HIs, which dominates the near-field part for $\varphi \lesssim 0.08$, and the scaling relation, $q_m \propto \varphi^{1/3}$, valid in low-salinity systems for the wavenumber location of the structure factor peak (Banchio & Nägele, 2008). As a consequence, the $\varphi^{1/3}$ concentration dependence of K is observed both for dilute fluid and crystalline systems of charged particles.

The experimental results of Rojas-Ochoa (2004) for the low-salinity sedimentation coefficient of a suspension of charged polystyrene spheres in an ethanol/water mixture
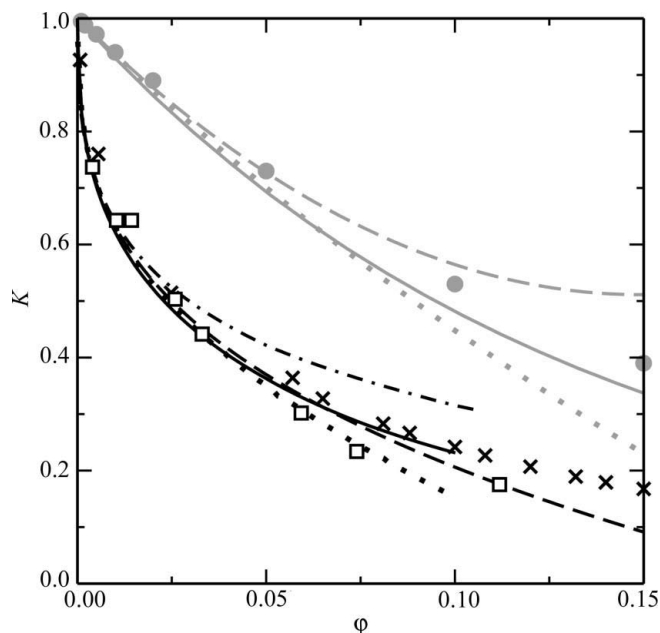

Figure 2
Sedimentation coefficient, $K = U_s/U_0$, of charged spheres at low salinity compared with that of neutral hard spheres. Experimental DLS/SLS data are shown for charged polystyrene spheres in an ethanol/water mixture (Rojas-Ochoa, 2004) (open squares) and for our TPM-coated silica spheres (crosses). Solid (dotted) black lines: $\delta\gamma$ theory (full PA scheme) results for the low-salinity polystyrene spheres system, obtained using the PBRMSA input for $S(q)$ with a fixed charge number $Z = 200$. Dashed–dotted black line: d_S-corrected $\delta\gamma$ scheme result. Dashed black line: scaling form $1 - 1.71\varphi^{1/3}$ according to equation (5). Gray filled circles: hard-sphere simulation results by Ladd (1990). Dashed gray line: second-order virial result for HS given in equation (8). Solid (dotted) gray lines: $\delta\gamma$ scheme (full PA scheme) results for HS with Percus–Yevick input for $S(q)$.

($a = 58.7$ nm, $n_s = 1\,\mu M$, $L_B = 1.48$ nm), and also our data for the charged silica spheres system, are in accord with the OMF-based prediction of a steep (as compared to neutral spheres) $\varphi^{1/3}$-like decay of the sedimentation coefficient. The experimental values of K in both systems discussed in Fig. 2 have been deduced from small-q DLS and static light scattering (SLS) measurements of $D(q)$ and $S(q)$, extrapolated to $q = 0$. Therefore, there is an unavoidable scatter in the extrapolated data, in particular considering that the osmotic compressibility coefficient $S(0)$ of low-salinity systems is very small.

In contrast to charged particles, the small-φ dependence of K is well represented for neutral spheres by a regular virial expansion. In fact, the second-order virial expression in equation (8) coincides, for $\varphi \lesssim 0.08$, with the simulation data for K^{HS} reported by Ladd (1990). At larger φ, shielding arising from the higher-order HI terms comes into play, contributing to K through the higher-order virial coefficients. Since shielding is disregarded in the full PA scheme, it notably overestimates the strength of the HIs for $\varphi \gtrsim 0.1$. When applied to concentrations beyond its range of applicability, too small and eventually even nonphysical negative values for K are predicted (see the dotted lines in Fig. 2). The reason for the failure of the full PA scheme at higher φ is that it approximates the many-sphere hydrodynamic mobility matrix in a way that does not guarantee the positive definiteness of this matrix for all physically allowed particle configurations.

Fig. 2 displays additionally, both for neutral spheres and for the system parameters of the charged polystyrene spheres system (Rojas-Ochoa, 2004), the predictions for K by the $\delta\gamma$ scheme of Beenakker & Mazur (1984) and by the full PA scheme. The theoretical predictions for the silica system are not shown in order to not overburden the figure with too many curves.

For neutral hard spheres, in both analytical methods, the Percus–Yevick solution for $S(q)$ is used as input. To leading order in φ, we have obtained numerically that $K_{PA}^{HS} = 1 - 6.546\varphi$, in full agreement with the first-order coefficient in equation (8). For comparison, $K_{\delta\gamma}^{HS} = 1 - 7.339\varphi + \mathcal{O}(\varphi^2)$. Thus, the $\delta\gamma$ scheme underestimates somewhat the hard-sphere sedimentation coefficient at small φ. It is less accurate than the PA scheme at small φ owing to its incomplete account of two-body HI contributions, notably its neglect of lubrication, which plays a role for neutral spheres. Lubrication occurs in the thin fluid layer between two almost touching spheres in a relative squeezing or shearing motion. It is more influential to self-diffusion than to sedimentation, since in the latter case the (monodisperse) spheres move with equal mean velocities in the direction of the applied force field. In self-diffusion, on the other hand, a tagged particle is thermodynamically driven in a squeezing motion towards particles in front of it. At larger φ, however, the $\delta\gamma$ scheme prediction for K^{HS} is closer to the simulation data than the full PA scheme result. We attribute this to the approximate inclusion of many-body HIs into the $\delta\gamma$ scheme which describe hydrodynamic shielding.

For charged spheres and small φ, the full PA scheme result for K follows precisely the scaling prediction $1 - a_s \varphi^{1/3}$, with

$a_s = 1.71$. The (uncorrected) $\delta\gamma$ scheme captures the overall φ dependence of K at least in a qualitative way, regarding both the two considered charge-stabilized systems and neutral hard spheres. Extensive comparisons with lower-q ASD simulation data of $H(q)$ (a representative example is shown in §3.4), show that the $\delta\gamma$ scheme has the tendency to somewhat underestimate K. The self-part-corrected $\delta\gamma$ scheme, on the other hand, overestimates $K \simeq H(q \ll q_m)$. At larger q values, however, including the principal peak region of $H(q)$, it is in distinctly better agreement with the simulation data for $H(q)$ than the uncorrected version (Banchio & Nägele, 2008). Indeed, the self-part-corrected $\delta\gamma$ scheme result in Fig. 2 for charged polystyrene spheres, with the d_S input calculated using the full PA scheme, lies distinctly above the experimental data for K. For the parameters of the polystyrene system, a least-squares fit of the calculated sedimentation coefficients in the range $\varphi \leq 0.02$ leads to equation (5), with coefficients $a_s = 1.65$, 1.75 and 1.71 for the d_S-corrected and uncorrected $\delta\gamma$ schemes, and the full PA scheme, respectively. In accord with the general trends discussed above, the full PA scheme result for K, which becomes exact at low φ, is bracketed by the self-part-corrected and -uncorrected $\delta\gamma$ scheme predictions.

3.3. Diffusion function

We proceed by discussing the short-time diffusion function, $D(q)$, defined in equation (2), which is measured in short-time DLS and XPCS experiments. DLS data of its inverse, $d_0/D(q)$, are included in the bottom part of Fig. 3, for a low-salinity system of charged silica spheres at a volume fraction $\varphi = 0.15$ rather close to the freezing transition value. The experimental data are compared with our ASD simulation result for $D(q)$, the (d_S-corrected) $\delta\gamma$ scheme result where the d_S part is taken from the ASD simulation, and the full PA scheme prediction. For the two analytic schemes, the PBRMSA input for $S(q)$ shown in the top part of Fig. 3 was used.

The shape of $d_0/D(q)$ is similar to that of $S(q)$, since $d_0/D(q) = S(q)/H(q)$ according to equation (2). The analytical PBRMSA scheme predicts a structure factor in excellent agreement with our MC simulation data and with the $S(q)$ obtained from the numerically elaborate RY scheme. The excellent agreement between all $S(q)$ depicted in the top part of Fig. 3, for all displayed wavenumbers, points to the accuracy of our scattering data. The only adjustable parameter in calculating $S(q)$ has been the effective charge number, uniquely determined as $Z = 190$ by the PBRMSA, RY and MC methods, from matching the experimental $S(q_m)$.

We recall from equation (2) that $D(q \to \infty) = d_S$ and $D(q \to 0) = d_0 K / S(q \to 0) = d_c$. Here, d_c is the short-time collective diffusion coefficient, which quantifies the initial decay rate of long-wavelength thermal concentration fluctuations. The short-time d_c is only slightly larger than its long-time counterpart, even when a concentrated system is considered. The relative osmotic compressibility coefficient, $S(q \to 0)$, in the considered low-salinity system is very small, so that d_c is much larger than d_0, reflected in Fig. 3 by the low-

q values of $d_0/D(q)$ being close to zero. The function $D(q)$ attains its minimum at q_m. The so-called cage diffusion coefficient, $D(q_m)$, characterizes the slow relaxation of density fluctuations of a wavelength $\sim 2\pi/q_m$, matching the radius of the nearest-neighbor shell. With increasing concentration and pair interactions, the cage stiffens, *i.e.* it becomes more sharply structured, as reflected by a smaller $D(q_m)$.

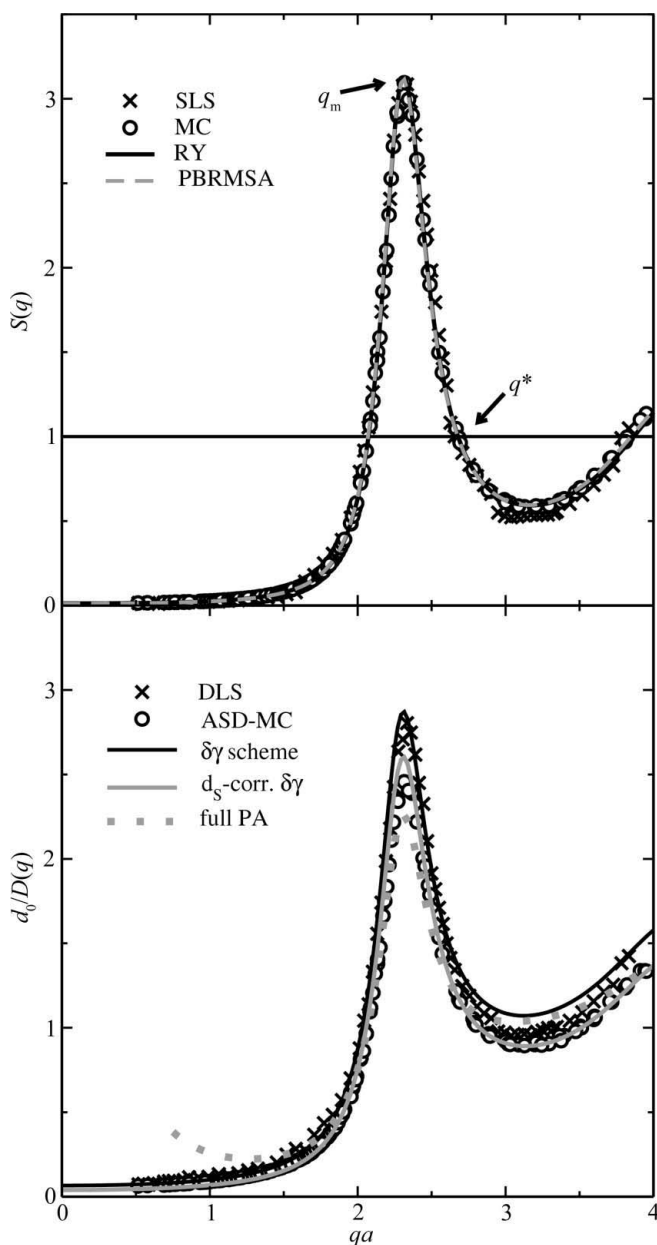According to the bottom part of Fig. 3, there is good agreement between the ASD simulation data for $d_0/D(q)$ and the d_S-corrected $\delta\gamma$ scheme prediction with its PBRMSA input. The ASD simulation peak height is somewhat overestimated by the uncorrected $\delta\gamma$ scheme, which uses too small a value for the self-diffusion coefficient of charged spheres (see Fig. 1). For the charged silica particles system considered here, the experimental peak height of $d_0/D(q)$ happens to be somewhat closer to that of the uncorrected $\delta\gamma$ scheme. However, the first minimum of $d_0/D(q)$ to the right of q_m is in better accord with the corrected $\delta\gamma$ scheme prediction.

To illustrate the failure of the full PA scheme for concentrations $\varphi \gtrsim 0.1$ where many-body HIs are strong, we have included its prediction in Fig. 3. It deviates from the experimental and simulation data most strongly at $q \simeq 0$ and near q_m, reflecting its overestimation of the HIs at the large volume fraction $\varphi = 0.15$, by giving too small a value for K and too large a value for $H(q_m)$.

3.4. Hydrodynamic function

In Fig. 4 the experimental findings of Philipse & Vrij (1988) for the $H(q)$ and $S(q)$ of a well structured, charge-stabilized suspension of silica spheres suspended in a 70:30 toluene/ethanol mixture ($\varepsilon = 10$ at $T = 298$ K), are compared with our theoretical and simulation predictions based on the OMF model. The PBRMSA, RY and MC $S(q)$ of common charge number $Z = 100$, shown in the inset, almost coincide in the depicted q range, demonstrating the accuracy of the PBRMSA scheme.

Figure 3
Top: static structure factor, $S(q)$, obtained by SLS (crosses) and compared with PBRMSA and RY results (lines), and MC simulation data (open circles) for a common $Z = 190$. Bottom: short-time inverse diffusion function, $d_0/D(q)$, for a low-salinity system of charged silica spheres. Crosses: DLS data. Open circles: ASD–MC simulation data. Solid black and gray lines: uncorrected and d_S-corrected $\delta\gamma$ scheme predictions, respectively. Dotted gray line: full PA method result. The system parameters are $a = 136$ nm, $\varphi = 0.15$, $n_s = 0.7$ μM and $L_B = 8.64$ nm.
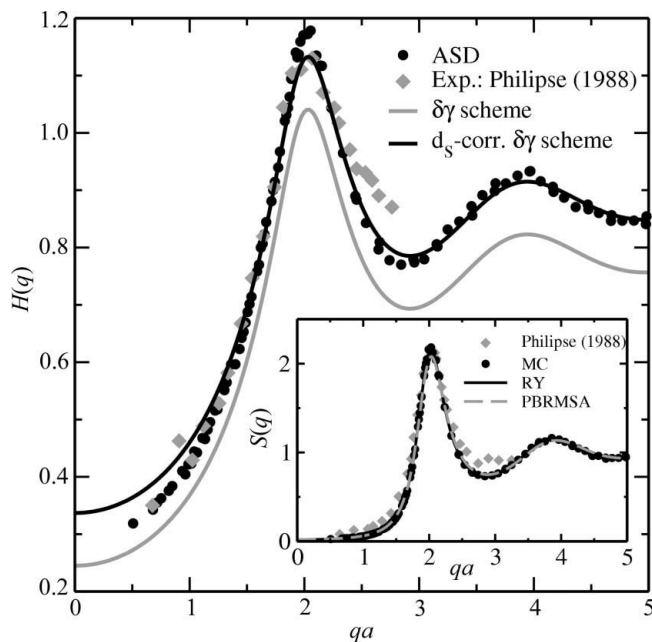

Figure 4
Gray diamonds: DLS and SLS data for $H(q)$ and $S(q)$ (in inset), respectively, taken from Philipse & Vrij (1988), for a charge-stabilized system at $\varphi = 0.101$, in comparison with corresponding ASD and MC data predictions (filled black circles). Solid gray and black lines: uncorrected and d_S-corrected $\delta\gamma$ scheme results, respectively. Black solid and dashed gray lines in inset: RY and PBRMSA $S(q)$, respectively, for $Z = 100$, $a = 80$ nm, $n_s = 2$ μM and $L_B = 5.62$ nm.

There is good overall agreement between the experimental $H(q)$ and the ASD and d_S-corrected $\delta\gamma$ scheme results (with d_S taken from the ASD simulation), on accounting for the scatter in the experimental data for $H(q)$, which has been obtained from multiplying the experimental data for $D(q)$ by those for $S(q)$. The d_S-corrected $\delta\gamma$ scheme underestimates to some extent the ASD $H(q_m)$, but except for the precise peak value the overall shape of $H(q)$ is well reproduced. Without d_S correction, the ASD $H(q)$ is underestimated at all q, owing to the fact that the $\delta\gamma$ scheme predicts too small a value for the charged-particle d_S. Figs. 3 and 4 exemplify that the (self-part-corrected) $\delta\gamma$ scheme allows for predicting consistently, and to almost quantitative accuracy, the short-time generic features of many charge-stabilized systems including small proteins and large colloidal spheres.

Low-salinity systems are typically characterized by a peak value of $H(q_m)$ larger than one. In a recent study based on the OMF model, the upper limiting freezing line for $H(q_m)$ was derived (Gapinski *et al.*, 2010), from which it follows that $H(q_m)$ never exceeds the value of 1.3. However, $H(q_m)$ in low-salt systems is not always larger than one. At very low φ, it increases monotonically according to $1 + p_m\varphi^{1/3}$, with a moderately system-dependent coefficient $p_m > 0$ [see equation (7)]. At larger φ where near-field HIs matter, $H(q_m)$ can pass through a maximum typically occurring at $\varphi \simeq 10^{-2}$–10^{-1}, with an ensuing decline when φ is further increased. Provided the system remains fluid at larger φ, such as in apoferritin protein solutions (Gapinski *et al.*, 2005), $H(q_m)$ can reach values smaller than one.

In the OMF model, $H(q_m)$ is bound from below by the corresponding peak height of neutral spheres. The latter decreases linearly in φ in the whole fluid phase regime [see equation (10)]. At fixed φ and with increasing salt content, $H(q_m)$ and d_S decrease monotonically, with q_m shifted to larger q values, towards the limiting hard-sphere values $H^{HS}(q_m)$ and d_S^{HS}, respectively. Opposite to this, K increases monotonically with increasing salinity, for the reasons discussed earlier, towards its upper hard-sphere limit. In summary, the ordering relations

$$H(q_m) \geq H^{HS}(q_m), \quad d_S \geq d_S^{HS}, \quad K \leq K^{HS}, \qquad (11)$$

are fulfilled. The equality sign holds for zero particle charge, $Z = 0$, and in the infinite salinity limit, $\kappa a \to \infty$. The OMF model ordering relations in equation (11) are obeyed by a wide variety of experimentally studied charge-stabilized systems, including nanosized proteins (Gapinski *et al.*, 2005), suspensions of compact colloidal particles (Philipse & Vrij, 1988; Phalakornkul *et al.*, 1996; Härtl *et al.*, 1999; Rojas-Ochoa, 2004; Rojas-Ochoa *et al.*, 2003; Gapinski *et al.*, 2009; Banchio *et al.*, 2006; Holmqvist & Nägele, 2010) and thermosensitive charged microgel spheres (Braibanti *et al.*, 2010).

In a series of articles, Robert, Grübel and coworkers (Grübel *et al.*, 2008; Robert, 2007; Riese *et al.*, 2000; Robert *et al.*, 2008) reported their observation of very small values for $H(q)$ for certain low-salinity suspensions of intermediately large volume fractions, which they studied by combining XPCS and SAXS techniques. At all probed wavenumbers,

their $H(q)$ are substantially smaller than those of neutral hard spheres at the same φ. This finding of so-called ultra-small $H(q)$ is incompatible with the OMF model since the first two ordering relations in equation (11) are violated.

A typical result for an ultra-small $H(q)$ with peak height $H(q_m) \simeq 0.47$, taken from Robert *et al.* (2008) for a system of poly(perfluoropentyl methacrylate) spheres in a water/glycerol mixture at $\varphi = 0.18$, is shown in Fig. 5, in comparison with our OMF model-based simulation and theoretical results for $H(q)$, which predict a peak value for $H(q)$ larger than one. The inset displays the experimentally determined $S(q)$, and the peak-height-adjusted MC, RY and PBRMSA results obtained for the common charge value $Z = 163$ and $n_s = 16\,\mu M$ ($\kappa a = 1.46$). The experimental peak height, $S(q_m) \simeq 2.63$, identifies the system as fluid-ordered according to the Hansen–Verlet freezing rule. There is a visible small-q upturn in the experimental $S(q)$ which is not reproduced by the OMF structure factors describing purely repulsive particles. However, this upturn should not be over-interpreted as a sign of a significantly influential particle attraction since the experimental $S(q)$ of very similar systems of charged poly-(perfluoropentyl methacrylate) spheres reported by Robert *et al.* (2008) do not have such an upturn. Moreover, the peak position of the experimental $S(q)$ in Fig. 5 fulfills the relation $q_m = 1.1 \times 2\pi n^{1/3}$ (Banchio & Nägele, 2008), characteristic of a low-salinity system of electrostatically strongly repelling particles where van der Waals attraction plays no role. This
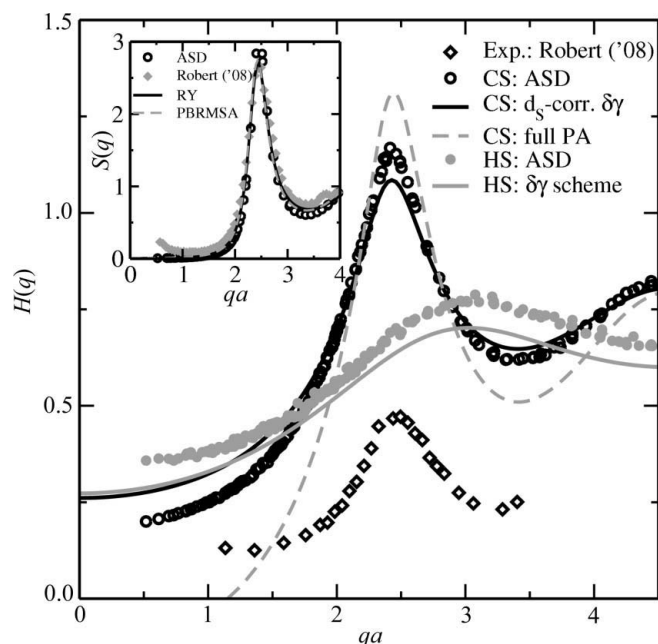

Figure 5
XPCS and SAXS data of $H(q)$ and $S(q)$ (in inset), taken from Robert *et al.* (2008), for a low-salinity system of charged poly(perfluoropentyl methacrylate) spheres (CS) with $a = 62.5$ nm, $n_s = 16\,\mu M$ and $\varphi = 0.18$ in a water/glycerol mixture at $T = 293$ K, where $\varepsilon = 62.95$ and $L_B = 0.91$ nm (open diamonds). Inset: RY and PBRMSA $S(q)$ for $Z = 163$. Comparison with OMF model-based ASD data, d_S-corrected $\delta\gamma$ and full PA scheme results for $H(q)$, all obtained using $Z = 163$. The experimental $H(q)$ is substantially smaller than the ASD $H^{HS}(q)$ (gray circles) and the $\delta\gamma$ scheme result for hard spheres (gray solid line).

follows also from standard DLVO theory when the parameters for the electric potential part quoted in the caption of Fig. 5 are used.

Just like in the silica system considered previously, the d_S-corrected $\delta\gamma$ scheme result for $H(q)$, based on the PBRMSA $S(q)$ input for its distinct part depicted in the inset, and the precise ASD simulation result for its self-part, is in overall good agreement with the full ASD simulation result for $H(q)$. It underestimates the ASD peak height to some extent, but aside from the precise peak value the agreement with the ASD $H(q)$ is quantitatively good.

For completeness, Fig. 5 shows also the full PA scheme prediction for $H(q)$. The concentration here is clearly too large for the full PA scheme to apply, with the consequence that nonphysical negative values of $H(q)$ are predicted for $qa \lesssim 1.2$. This shows that for the present system, where $\varphi = 0.18$, $H(q)$ is strongly influenced by many-body HIs. Quite notably, however, for the same particle system, an ultra-small hydrodynamic function, with $H(q_m) \simeq 0.7 < H^{HS}(q_m) = 0.95$, was reported by Robert *et al.* (2008) at $\varphi = 0.04$, *i.e.* for a concentration where two-body HIs dominate.

The experimental peak height in Fig. 5 is considerably smaller than the peak value, $H^{HS}(q_m) = 0.76$, of hard spheres, the latter calculated according to equation (10). To allow for a comparison at all probed q values, Fig. 5 includes the ASD and $\delta\gamma$ scheme results for the $H(q)$ of hard spheres. The hard-sphere structure factor peak value is $S^{HS}(q_m) = 1.19$ at $\varphi = 0.18$.

Grübel, Robert and coworkers originally tried to explain their observation of strikingly low values for $H(q)$ as the result of HI screening (Riese *et al.*, 2000; Robert, 2001). To support their assertion, they presented a Brinkman fluid-type calculation of $H(q)$ (Riese *et al.*, 2000), wherein only the leading-order far-field part of the hydrodynamic pair mobility is considered, treating the Brinkman screening length as a fitting parameter. However, in a later experimental–theoretical study (Banchio *et al.*, 2006), it was pointed out that hydrodynamic screening does not occur in fluid-ordered, unconfined suspensions of mobile colloidal particles (see here also Diamant, 2007). Furthermore, the assumed screening of the HIs conflicts with the fact that the short-time diffusion and viscosity properties of many charge-stabilized systems, at concentrations and interaction parameters similar to those probed by Robert and co-workers, are well explained by OMF model-based methods without any necessity to invoke HI screening. The low-salinity system in Fig. 3, for example, is in the concentration range where an ultra-slow $H(q)$ should be observable.

More recently, Robert and co-workers retracted their interpretation of ultra-small $H(q)$ as being due to HI screening (Hammouda & Mildner, 2007). In an alternative attempt to explain their findings (Robert *et al.*, 2008), they introduced a correction factor, $f = \eta_0/\eta_{eff} < 1$, multiplying the OMF model-based $\delta\gamma$ scheme $H(q)$, with the value of f determined such that the ultra-small experimental $H(q)$ is matched overall. Furthermore, they conjecture that f can be identified by the ratio of the solvent viscosity and some effective

suspension viscosity η_{eff}, leaving it unspecified, however, whether η_{eff} should be identified with the high-frequency viscosity, η_∞, or with the substantially larger static suspension viscosity. This *ad-hoc* modification of the $\delta\gamma$ scheme lacks a sound physical basis, since the $\delta\gamma$ scheme expression for $H(q)$ describes a genuine diffusion property. The values for f obtained from fitting the ultra-small $H(q)$ given by Robert *et al.* (2008) are consistent with neither calculated (Banchio & Nägele, 2008) nor experimental (Bergenholtz *et al.*, 1998) results for η_0/η_∞. In this context, we note that the generalized Stokes–Einstein relation, $[D(q_m)/d_0](\eta_\infty/\eta_0) \simeq 1$, relating the cage diffusion coefficient to the short-time (high-frequency) viscosity, is valid approximately for neutral spheres only (Banchio & Nägele, 2008; Abade *et al.*, 2010c,d) but not for low-salinity suspensions of charge-stabilized particles (Koenderink *et al.*, 2003; Banchio & Nägele, 2008).

3.5. Influence of additional interactions

In the following, we analyze the effect on $H(q)$ caused by particle interaction contributions not considered in the OMF model. On a qualitative level, we discuss the influence of particle porosity, residual attractive forces and microion kinetics on the shape of $H(q)$.

The effect of particle porosity on the $H(q)$ of dense suspensions of neutral porous spheres has been explored in a recent simulation study (Abade *et al.*, 2010a,b). A nonzero solvent permeability has the effect of weakening the HIs, thus reducing the deviations of $H(q)$ at all q from its zero-concentration limiting value of one. For the same reason, a suspension of porous particles is less viscous than a suspension of impermeable ones (Abade *et al.*, 2010c,d). Porosity is less influential when the particles are charged, since near-contact configurations are then unlikely. The particles studied by Robert *et al.* are only very weakly porous, if at all. Thus, porosity cannot explain the ultra-small $H(q)$s. Conversely, significant porosity would lead to an overall $H(q)$ closer to one.

An attractive interaction contribution enlarges both $S(0)$ and the sedimentation coefficient K (Moncha-Jordá *et al.*, 2010). The enlargement of the latter is overcompensated by the former, at least at smaller φ (van den Broeck *et al.*, 1981). Thus, in dispersions of moderately charged particles, such as bovine serum albumin or lysozyme proteins with sufficiently strong short-range attraction, the collective diffusion coefficient, $d_c = d_0 K/S(0)$, can attain values smaller than d_0 (Cichocki & Felderhof, 1990; Bowen & Mongruel, 1998; Bowen *et al.*, 2000; Prinsen & Odijk, 2007).

Opposite to sedimentation, attraction tends to slow self-diffusion, resulting in smaller values of the short-time and long-time self-diffusion coefficients (Cichocki & Felderhof, 1990; Seefeldt & Solomon, 2003). Attraction-induced slowing of self-diffusion is accompanied by an augmentation of the short-time (high-frequency) and long-time (static) suspension viscosities (Woutersen *et al.*, 1994). Attraction fosters the formation of short-lived, transient particle pairs and clusters, which are better shielded from the solvent backflow so that

sedimentation is enhanced. In self-diffusion, however, the mean velocity of a weakly forced particle driven towards its next-neighbor cage particles becomes smaller with increasing attraction, owing to the greater tendency of nearby particles to form a transient cluster. This picture also explains why attraction-induced slowing of long-time self-diffusion is found not only in colloidal systems, where HIs are present, but also in atomic liquids (Bembenek & Szamel, 2000). Sedimentation is different in the sense that all particles, not just a single tagged one, are forced to move, on average, in the direction of the external force. Summarizing, the overall effect of attraction is to lower the difference $H(\infty) - H(0)$ and to shift the peak position q_m to larger values.

The data reported by Robert and co-workers for $S(q)$ and $H(q)$ give no hint of an appreciable attractive interaction part. The short-range van der Waals attraction acting between the particles is masked in low-salinity systems by the strong and long-ranged electric forces to such an extent that it cannot influence $H(q)$ significantly. Moreover, the experimental $S(q)$ given by Robert and co-workers can be described to good accuracy by the OMF model-based structure factor. Significant attraction would enlarge at low q the gap between the OMF model and the ultra-small $H(q)$ in Fig. 5, instead of reducing it.

On first sight, the non-instantaneous electrokinetic relaxation of counter- and co-ions forming overlapping electric double layers around the charged colloids is a more promising candidate for causing ultra-small $H(q)$. Indeed, the relaxation of the microion clouds has a slowing influence on colloid diffusion, referred to as the electrolyte friction effect. This effect can lower $H(0)$ (Gapinski et al., 2005) to a smaller extent, and also the values of the short-time and long-time self-diffusion coefficients (McPhie & Nägele, 2007). However, electrolyte friction scales with the ratio, d_0/d_m, of the free diffusion coefficient, d_0, of the slowly moving colloids relative to the (mean) free diffusion coefficient, d_m, of the small microions (Retailleau et al., 1999; Gapinski et al., 2005; McPhie & Nägele, 2007). Because of the huge difference in these two free diffusion coefficients, it is unlikely that electrokinetics can explain the strikingly low values for $H(q)$ reported by Robert and collaborators. Whereas the electrokinetic influence on colloid diffusion is very small for larger colloidal spheres, it can be significantly strong for small, nanosized macroions such as proteins.

4. Conclusions

The generic behavior of short-time diffusion properties in suspensions of charge-stabilized colloidal particles with strong electrostatic interactions has been studied by simulation and analytical theory, in conjunction with dynamic light scattering on charged silica spheres. Our calculations are based on the OMF model, which interpolates between the limiting cases of a deionized (low-salinity) system and a system of neutral hard spheres. Two analytical methods to determine $H(q)$, namely the full PA scheme and the (self-part-corrected) $\delta\gamma$ scheme, have been tested against Stokesian dynamics simulations and

compared with experimental results. The full PA scheme becomes exact at very low volume fractions but it cannot be applied to denser systems. The self-part-corrected $\delta\gamma$ scheme gives overall good results in the whole liquid phase regime, for all wavenumbers except those in the low-q regime. The experimental confirmation of OMF model-based low-φ predictions, notably the $\varphi^{1/3}$ scaling of K (Rojas-Ochoa, 2004) and $H(q_m)$ (Härtl et al., 1999), the $\varphi^{4/3}$ scaling of d_S/d_0 (Overbeck et al., 1999; Holmqvist & Nägele, 2010) and in addition the $d_S^r/d_0^r = 1 - a_r\varphi^2$ scaling (with $a_r \simeq 1.3$) of the short-time rotational diffusion coefficient d_S^r, normalized by its zero-concentration limiting value d_0^r (Koenderink et al., 2003), add to the credibility of the OMF model.

A large body of experimental results for $D(q)$ and $H(q)$, for systems of different particle types and sizes, concentrations, salt contents, and solvents, is well described by the OMF model, with all the ordering relations in equation (11) satisfied. Residual attractive-pair interactions or particle porosity, and most likely also electrolyte friction, cannot explain the ultra-small $H(q)$ findings of Robert and collaborators. Ultra-small values of $H(q)$ have not been observed in our scattering experiments, nor in those by our collaborators and various other groups (Philipse & Vrij, 1988; Phalakornkul et al., 1996; Rojas-Ochoa et al., 2003; Rojas-Ochoa, 2004).

Information on short-time dynamic properties is indispensable for a better understanding of long-time dynamic properties such as the static viscosity and the long-time self-diffusion coefficient. Short-time transport coefficients are used, for example, as input in mode-coupling and dynamic density functional theory calculations of long-time properties. For charge-stabilized systems, we have shown recently (Holmqvist & Nägele, 2010) that d_S and $D(q)$ are linked to their corresponding long-time quantities by a simple, approximate scaling relation.

References

Abade, G., Cichocki, B., Ekiel-Jezewska, M., Nägele, G. & Wajnryb, E. (2010a). J. Chem. Phys. **132**, 014503.

Abade, G., Cichocki, B., Ekiel-Jezewska, M., Nägele, G. & Wajnryb, E. (2010b). Phys. Rev. E, **81**, 020401.

Abade, G., Cichocki, B., Ekiel-Jezewska, M., Nägele, G. & Wajnryb, E. (2010c). J. Phys. Condens. Matter, **22**, 322101.

Abade, G., Cichocki, B., Ekiel-Jezewska, M., Nägele, G. & Wajnryb, E. (2010d). J. Chem. Phys. **133**. In the press.

Banchio, A. J. & Brady, J. (2003). J. Chem. Phys. **118**, 10323–10332.

Banchio, A. J. Gapinski, J., Patkowski, A., Häussler, W., Fluerasu, A., Saccana, S., Holmqvist, P., Meier, G., Lettinga, M. & Nägele, G. (2006). Phys. Rev. Lett. **96**, 138303.

Banchio, A. J., McPhie, M. & Nägele, G. (2008). J. Phys. Condens. Matter, **20**, 404213.

Marco Heinen et al. · Short-time diffusion of charge-stabilized particles **979**

Banchio, A. J. & Nägele, G. (2008). *J. Chem. Phys.* **128**, 104903.

Banchio, A. J., Nägele, G. & Bergenholtz, J. (1999). *J. Chem. Phys.* **111**, 8721–8740.

Beenakker, C. & Mazur, P. (1984). *Physica A*, **126**, 349–370.

Bembenek, S. & Szamel, G. (2000). *J. Phys. Chem. B*, **104**, 10647–10652.

Bergenholtz, J., Horn, F., Richtering, W., Willenbacher, N. & Wagner, N. (1998). *Phys. Rev. E*, **58**, R4088–R4091.

Bowen, W., Liang, Y. & Williams, P. (2000). *Chem. Eng. Sci.* **55**, 2359–2377.

Bowen, W. & Mongruel, A. (1998). *Colloids Surfaces A*, **138**, 161–172.

Braibanti, M., Heinen, M., Haro-Perez, C., Rojas-Ochoa, L., Nägele, G. & Trappe, V. (2010). In preparation.

Broeck, C. van den, Lostak, F. & Lekkerkerker, H. (1981). *J. Chem. Phys.* **74**, 2006–2010.

Cichocki, B., Ekiel-Jezewska, M., Szymczak, P. & Wajnryb, E. (2002). *J. Chem. Phys.* **117**, 1231–1241.

Cichocki, B., Ekiel-Jezewska, M. & Wajnryb, E. (1999). *J. Chem. Phys.* **111**, 3265–3273.

Cichocki, B. & Felderhof, B. (1990). *J. Chem. Phys.* **93**, 4427–4432.

Diamant, H. (2007). *Isr. J. Chem.* **47**, 225–231.

Gapinski, J., Patkowski, A., Banchio, A. J., Buitenhuis, J., Holmqvist, P., Lettinga, M., Meier, G. & Nägele, G. (2009). *J. Chem. Phys.* **130**, 084503.

Gapinski, J., Patkowski, A., Banchio, A. J., Holmqvist, P., Meier, G., Lettinga, M. & Nägele, G. (2007). *J. Chem. Phys.* **126**, 104905.

Gapinski, J., Patkowski, A. & Nägele, G. (2010). *J. Chem. Phys.* **132**, 054510.

Gapinski, J., Wilk, A., Patkowski, A., Häussler, W., Banchio, A. J., Pecora, R. & Nägele, G. (2005). *J. Chem. Phys.* **123**, 054708.

Grübel, G., Madsen, A. & Robert, A. (2008). *X-ray Photon Correlation Spectrocsopy (XPCS) in Soft-Matter Characterization.* Berlin: Springer-Verlag.

Hammouda, B. & Mildner, D. F. R. (2007). *J. Appl. Cryst.* **40**, 250–259.

Härtl, W., Beck, C. & Hempelmann, R. (1999). *J. Chem. Phys.* **110**, 7070–7072.

Heinen, M., Banchio, A. & Nägele, G. (2010). *J. Chem. Phys.* Submitted.

Holmqvist, P. & Nägele, G. (2010). *Phys. Rev. Lett.* **104**, 058301.

Jeffrey, D. & Onishi, Y. (1984). *J. Fluid Mech.* **139**, 261–290.

Jones, R. & Schmitz, R. (1988). *Physica A*, **149**, 373–394.

Kim, S. & Mifflin, R. (1985). *Phys. Fluids*, **28**, 2033–2045.

Koenderink, G., Zhang, H., Aarts, D., Lettinga, M., Philipse, A. & Nägele, G. (2003). *Faraday Discuss.* **123**, 335–354.

Ladd, A. (1990). *J. Chem. Phys.* **93**, 3484–3494.

McPhie, M. & Nägele, G. (2007). *J. Chem. Phys.* **127**, 034906.

Moncha-Jordá, A., Louis, A. & Padding, J. (2010). *Phys. Rev. Lett.* **104**, 068301.

Nägele, G. (1996). *Phys. Rep.* **272**(5–6), 215–372.

Nägele, G., Mandl, B. & Klein, R. (1995). *Prog. Colloid. Polym. Sci.* **98**, 117–123.

Nägele, G., Steininger, B., Genz, U. & Klein, R. (1994). *Phys. Scr. T*, **55**, 119–126.

Overbeck, E., Sinn, C. & Watzlawek, M. (1999). *Phys. Rev. E*, **60**, 1936–1939.

Phalakornkul, J., Gast, A., Pecora, R., Nägele, G., Ferrante, A., Mandl-Steininger, B. & Klein, R. (1996). *Phys. Rev. E*, **54**, 661–675.

Philipse, A. P. & Vrij, A. (1988). *J. Chem. Phys.* **88**, 6459–6470.

Prinsen, P. & Odijk, T. (2007). *J. Chem. Phys.* **127**, 115102.

Pusey, P. (1978). *J. Phys. A*, **11**, 119–135.

Pusey, P. (1991). *Liquids, Freezing and the Glass Transition.* Amsterdam: Elsevier.

Retailleau, P., Riès-Kautt, M., Ducruix, A., Belloni, L., Candau, S. & Munch, J. (1999). *Europhys. Lett.* **46**, 154.

Riese, D., Wegdam, G., Vos, W., Sprik, R., Fenistein, D., Bongaerts, J. & Grübel, G. (2000). *Phys. Rev. Lett.* **85**, 5460–5463.

Robert, A. (2001). PhD thesis, Université Joseph Fourier, Grenoble, France.

Robert, A. (2007). *J. Appl. Cryst.* **40**, s34–s37.

Robert, A., Wagner, J., Härtl, W., Autenrieth, T. & Grübel, G. (2008). *Eur. Phys. J. E*, **25**, 77–81.

Rogers, F. & Young, D. (1984). *Phys. Rev. A*, **30**, 999–1007.

Rojas-Ochoa, L. (2004). PhD thesis, Université de Fribourg, Switzerland.

Rojas-Ochoa, L., Vavrin, R., Urban, C., Kohlbrecher, J., Stradner, A., Scheffold, F. & Schurtenberger, P. (2003). *Faraday Discuss.* **123**, 385–400.

Seefeldt, K. & Solomon, M. (2003). *Phys. Rev. E*, **67**, 050402.

Segrè, P. & Pusey, P. (1996). *Phys. Rev. Lett.* **77**, 771–774.

Snook, I. & Hayter, J. (1992). *Langmuir*, **8**, 2280–2884.

Watzlawek, M. & Nägele, G. (1999). *J. Colloid Interface Sci.* **214**, 170–179.

Woutersen, A., Mellema, J., Blom, C. & de Kruif, C. (1994). *J. Chem. Phys.* **101**, 542–553.